Structural Engineering and Mechanics, *Vol. 57, No. 1 (2016) 45-63*
DOI: http://dx.doi.org/10.12989/sem.2016.57.1.045

Axial buckling response of fiber metal laminate circular cylindrical shells

Ali M. Moniri Bidgoli[1a] and Mohammad Heidari-Rarani[*2]

[1]*Faculty of Mechanical Engineering, College of Engineering, University of Tehran, 515-14395, Tehran, Iran*
[2]*Department of Mechanical Engineering, Faculty of Engineering, University of Isfahan, 81746-73441, Isfahan, Iran*

(Received September 22, 2014, Revised November 24, 2015, Accepted December 2, 2015)

Abstract. Fiber metal laminates (FMLs) represent a high-performance family of hybrid materials which consist of thin metal sheets bonded together with alternating unidirectional fiber layers .In this study, the buckling behavior of a FML circular cylindrical shell under axial compression is investigated via both analytical and finite element approaches. The governing equations are derived based on the first-order shear deformation theory and solved by the Navier solution method. Also, the buckling load of a FML cylindrical shell is calculated using linear eigenvalue analysis in commercial finite element software, ABAQUS. Due to lack of experimental and analytical data for buckling behavior of FML cylindrical shells in the literature, the proposed model is simplified to the full-composite and full-metal cylindrical shells and buckling loads are compared with the available results. Afterwards, the effects of FML parameters such as metal volume fraction (MVF), composite fiber orientation, stacking sequence of layers and geometric parameters are studied on the buckling loads. Results show that the FML layup has the significant effect on the buckling loads of FML cylindrical shells in comparison to the full-composite and full-metal shells. Results of this paper hopefully provide a useful guideline for engineers to design an efficient and economical structure.

Keywords: buckling; fiber metal laminate (FML); analytical modelling; finite element analysis

1. Introduction

Fiber metal laminates (FMLs) are created by adhesively combining thin sheets of monolithic materials with some types of reinforced prepreg as shown in Fig. 1. This material provides improved fatigue characteristics, considerable fire resistance, ductility, high specific stiffness and damage behavior (Sinmazçelik *et al*. 2011). Initial studies have shown that the use of this lightweight composite in the design of engineering components can lead to weight reduction up to 50% (Carrillo and Cantwell 2007). The concept of FML materials was first developed at the Delft University of Technology and FMLs, especially those based on a combination of 2024-T3 aluminum and S2-glass fibers are a class of composite materials that are growing in popularity for use in aerospace applications (Vlot *et al*. 2002). The most commercially available FMLs are

∗Corresponding author, Assistant professor, E-mail: m.heidarirarani@eng.ui.ac.ir
[a]M.Sc., E-mail: a.m.moniribidgoli@gmail.com

http://www.techno-press.org/?journal=sem&subpage=8 ISSN: 1225-4568 (Print), 1598-6217 (Online)

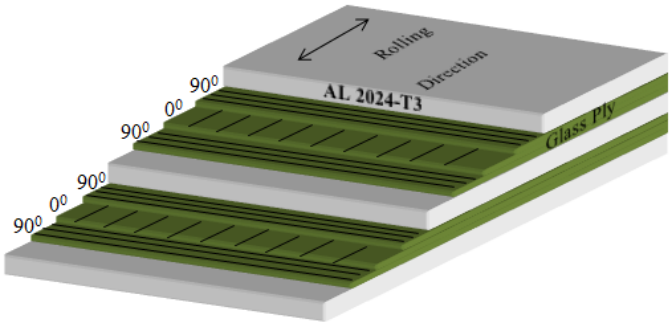

Fig. 1 Schematic of a GLARE 4B 3/2 layup

Table 1 Commercially available GLARE grades (Botelho *et al*. 2006)

Grade	Sub-grade	Metal type	Prepreg orientation in each composite layer
GLARE1	-	7475-T761	0˚/0˚
GLARE 2	GLARE 2A	2024-T3	0˚/0˚
	GLARE 2B	2024-T3	90˚/90˚
GLARE 3	-	2024-T3	0˚/90˚
GLARE 4	GLARE 4A	2024-T3	0˚/90˚/0˚
	GLARE 4B	2024-T3	90˚/0˚/90˚
GLARE 5	-	2024-T3	0˚/90˚/90˚/0˚
GLARE 6	GLARE 6A	2024-T3	+45˚/-45˚
	GLARE 6B	2024-T3	-45˚/+45˚

ARALL (Aramid Reinforced Aluminum Laminate) based on aramid fibers, GLARE (Glass Reinforced Aluminum Laminate) based on glass fibers and CARALL (Carbon Reinforced Aluminum Laminate) based on carbon fibers. Since FMLs are a relatively recent development, there is an absence of broad design base similar to that available for metal structure. Currently, FMLs such as GLARE and CARALL are attracting the interest of a number of aircraft manufacturers (Krishnakumar 1994). For example, GLARE is being used in the manufacture of the upper fuselage of the A380. Six standardized grades of GLARE are commonly being produced are shown in Table 1.

Due to the above advantages, cylindrical shells composed of FML materials can replace instead of the cylindrical shells made of full-metal or full-composite. As regards most of the cylindrical shells are used under axial loading and this loading may cause damage, therefore considering buckling load of this structure is necessary in the design process. Here is a difference between the "buckling load" and "critical buckling load". Buckling load is defined as the solution of eigenvalue problem so that a buckling load can be obtained for every eigenvalue. Critical buckling load is the minimum buckling loads caused the buckling behavior (Heidari-Rarani *et al*. 2014).

Reviewing the literature appear a large numbers of studies about the buckling behavior of full-metallic and full-composite cylindrical shells. For example, Mandal and Calladine (2000) investigated aspects of the elastic buckling of thin cylindrical shells under axial compression. Buckling behavior of elliptical cylindrical shells and tubes under compression is studied by Silvestre (2008) that a formulation of generalized beam theory developed to analysis the elastic

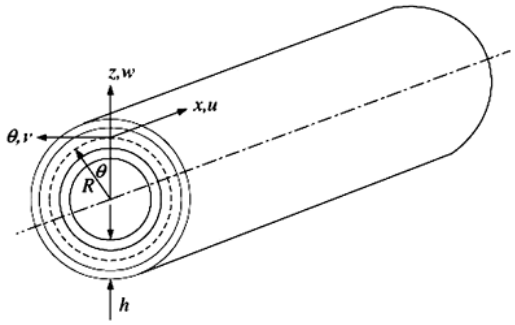

Fig. 2 Geometry and coordinate system of a cylindrical shell (Topal and Uzman 2009)

buckling behavior. Buckling of cross-ply circular cylindrical shells with various shell theories and simply-supported, clamped and free boundary conditions was studied by Khdeir *et al*. (1989). Kardomateas (1996) investigated three-dimensional elasticity solutions for the buckling of thick orthotropic cylindrical shells under axial compression and external pressure and shows the classical shell theories may produce highly non-conservative results on the critical loads. Buckling localization in a cylindrical panel under axial compression is studied by Tvergaard and Needleman (2000). Shen and Xiang (2008) studied buckling and post buckling of laminated cylindrical shells under combined axial compression and torsion based on the classical shell theory with Von-Karman Donnell type of kinematic nonlinearity. A new perturbation technique in numerical study on buckling of composite shells under axial compression is investigated by Tahir and Mandal (2012). Fan *et al*. (2015) obtained analytically the critical buckling load of cylindrical shells with stepwise variable wall thickness under axial compression.

Up to now, a few numbers of researchers have studied the buckling behavior of FML structures. The shear buckling behavior of the two FML panels, ARALL3 3/2 and GLARE 3 2/1, is investigated by Shi and Xiong (2000) using a probabilistic analysis method in order to predict the distributions of the buckling load. Also, Khalili *et al*. (2010) solved equilibrium equations for buckling, free and forced vibration problems of FML cylindrical shells using Galerkin method. However, to the knowledge of the authors, the buckling analysis of FML circular cylindrical shells using first-order shear deformation theory (FSDT) is not investigated yet. Therefore, the buckling loads of simply-supported FML circular cylindrical shells are analytically calculated based on the both classical lamination theory (CLT) and FSDT. Also, the buckling loads are estimated via finite element software, ABAQUS using linear eigenvalue analysis. The effects of different parameters of a FML are investigated on the buckling loads. Finally, the new interesting results are presented which provide a helpful insight for aircraft fuselage skin designers and space system engineers.

2. Governing equations

A FML circular cylindrical shell with mean radius R, thickness h, length L and the directions x, θ and z is shown in Fig. 2. According to the definition of FML, a coding system is used in this study for summarizing the name of FMLs. Each FML system is defined as "*FML name* (1+*i*)/*i*". For example, GLARE 3/2 defines a FML composed of three aluminum layers and two glass reinforced polymer prepreg. Also, the metal volume fraction (MVF) is defined as the sum of the

ratio of thicknesses of the individual aluminum layers to the total thickness of the laminate as $\mathrm{MVF}=\sum_{1}^{p} h_{al}/h$ where h_{al} is the thickness of each separate aluminum layer, h is the thickness of laminate and p is the number of aluminum layers (Vlot and Gunnink 2001). Hence, MVF=0 and MVF=1 represent full-composite and full-metal shells, respectively.

The equilibrium equations in cylindrical coordinates based on the FSDT for a cylindrical shell under axial loading can be expressed as the following simplified form (Li and Chen 2002)

$$\frac{\partial N_x}{\partial x}+\frac{\partial N_{x\theta}}{R\partial\theta}=0, \tag{1a}$$

$$\frac{\partial N_{x\theta}}{\partial x}+\frac{\partial N_{\theta}}{R\partial\theta}+\frac{Q_{\theta}}{R}=0, \tag{1b}$$

$$\frac{\partial Q_x}{\partial x}+\frac{\partial Q_{\theta}}{R\partial\theta}-\frac{N_{\theta}}{R}-N_a\frac{\partial^2 w_0}{\partial x^2}=0, \tag{1c}$$

$$\frac{\partial M_x}{\partial x}+\frac{\partial M_{x\theta}}{R\partial\theta}-Q_x=0, \tag{1d}$$

$$\frac{\partial M_{x\theta}}{\partial x}+\frac{\partial M_{\theta}}{R\partial\theta}-Q_{\theta}=0. \tag{1e}$$

where N_x, N_θ and $N_{x\theta}$ are force resultants; M_x, M_θ and $M_{x\theta}$ are moment resultants; Q_x and Q_θ are shear resultants and $\hat{N}$ is the axial force.

Stress-strain relationship for a cylindrical shell with N orthotropic layers and uniform thickness is as follows (Reddy 2003)

$$\begin{Bmatrix}\sigma_x\\ \sigma_\theta\\ \sigma_{z\theta}\\ \sigma_{xz}\\ \sigma_{x\theta}\end{Bmatrix}^{(k)}=\begin{bmatrix}\overline{Q}_{11} & \overline{Q}_{12} & 0 & 0 & \overline{Q}_{16}\\ \overline{Q}_{12} & \overline{Q}_{22} & 0 & 0 & \overline{Q}_{26}\\ 0 & 0 & \overline{Q}_{44} & \overline{Q}_{45} & 0\\ 0 & 0 & \overline{Q}_{45} & \overline{Q}_{55} & 0\\ \overline{Q}_{16} & \overline{Q}_{26} & 0 & 0 & \overline{Q}_{66}\end{bmatrix}\begin{Bmatrix}\varepsilon_x\\ \varepsilon_\theta\\ \varepsilon_{z\theta}\\ \varepsilon_{xz}\\ \varepsilon_{x\theta}\end{Bmatrix}^{(k)}, \tag{2}$$

where $\{\sigma\}$ and $\{\varepsilon\}$ are off-axis stresses and strains and $[\overline{Q}]$ is transformed stiffness matrix. With the integration of the stresses and moments on the entire multilayer, the resultant moments and forces will be achieved as follows (Vinson 1993)

$$\begin{Bmatrix}\{N\}\\ \{M\}\end{Bmatrix}=\begin{bmatrix}[A] & [B]\\ [B] & [D]\end{bmatrix}\begin{Bmatrix}\{\varepsilon^0\}\\ \{K\}\end{Bmatrix}, \tag{3a}$$

$$\{Q\} = [H]\begin{Bmatrix}\gamma_{\theta z}^{0}\\ \gamma_{xz}^{0}\end{Bmatrix}, \tag{3b}$$

$\{\varepsilon^0\}^T = \{\varepsilon_x^0, \varepsilon_\theta^0, \gamma_{x\theta}^0\}$ is the vector of the mid-surface engineering strains, $\{K\}^T = \{K_x, K_\theta, K_{x\theta}\}$ is the vector of the curvature and twist of the shell, [*A*], [*B*], [*D*] and [*H*] are the extensional, extension-bending coupling, bending and thickness shear stiffness matrices, respectively that are defined as follows (Nam *et al*. 2003)

$$\begin{aligned} A_{ij} &= \sum_{k=1}^{N} \overline{Q}_{ij}^{(k)}(z_{k+1}-z_k), \quad i,j=1,2,6 \qquad & B_{ij} &= \frac{1}{2}\sum_{k=1}^{N} \overline{Q}_{ij}^{(k)}(z_{k+1}^2-z_k^2), \quad i,j=1,2,6 \\ D_{ij} &= \frac{1}{3}\sum_{k=1}^{N} \overline{Q}_{ij}^{(k)}(z_{k+1}^3-z_k^3), \quad i,j=1,2,6 \qquad & H_{ij} &= k_s\sum_{k=1}^{N} \overline{Q}_{ij}^{(k)}(z_{k+1}-z_k), \quad i,j=4,5 \end{aligned} \tag{4}$$

where k_s is the shear correction factor introduced by Mindlin and is equal to 5/6 (Hosseini Hashemi *et al*. 2012).

Displacement field based on the FSDT are expressed as follows (Reddy 2003)

$$\begin{aligned} u(x,\theta,z) &= u_0(x,\theta) + z\phi_x(x,\theta), \\ v(x,\theta,z) &= v_0(x,\theta) + z\phi_\theta(x,\theta), \\ w(x,\theta,z) &= w_0(x,\theta), \end{aligned} \tag{5}$$

and the corresponding strain-displacement relations are:

$$\begin{gathered} \varepsilon_x^0 = \frac{\partial u_0}{\partial x}, \quad \varepsilon_\theta^0 = \frac{\partial v_0}{R\partial\theta} + \frac{w_0}{R}, \quad \gamma_{x\theta}^0 = \frac{\partial v_0}{\partial x} + \frac{1}{R}\frac{\partial u_0}{\partial\theta}, \quad \gamma_{\theta z}^0 = \frac{\partial w_0}{R\partial\theta} + \phi_\theta - \frac{v_0}{R}, \quad \gamma_{xz}^0 = \frac{\partial w_0}{\partial x} + \phi_x, \\ K_x = \frac{\partial\phi_x}{\partial x}, \quad K_\theta = \frac{\partial\phi_\theta}{R\partial\theta}, \quad K_{x\theta} = \frac{\partial\phi_\theta}{\partial x} + \frac{1}{R}\frac{\partial\phi_x}{\partial\theta}. \end{gathered} \tag{6}$$

where u_0, v_0 and w_0 are the displacement components of mid-plane in the axial, tangential and radial directions, respectively. Also, ϕ_x and ϕ_θ are the rotations of the normal to the mid-plane about θ- and x-directions, respectively. With substituting Eqs. (6) and (3) into Eq. (1), the governing equations in terms of displacement and rotation parameters can be obtained as follows

$$\frac{1}{R^2}\Bigg[R(B_{16}+B_{61})\left(\frac{\partial^2\phi_x(x,\theta)}{\partial x\partial\theta}\right) + R(B_{12}+B_{66})\left(\frac{\partial^2\phi_\theta(x,\theta)}{\partial x\partial\theta}\right) + R(A_{16}+A_{61})$$

$$\left(\frac{\partial^2 u_0(x,\theta)}{\partial x\partial\theta}\right) + R(A_{12}+A_{66})\left(\frac{\partial^2 v_0(x,\theta)}{\partial x\partial\theta}\right) + A_{11}\left(\frac{\partial^2 u_0(x,\theta)}{\partial x^2}\right)R^2 + B_{11}$$

$$\left(\frac{\partial^2\phi_x(x,\theta)}{\partial x^2}\right)R^2 + A_{12}R\left(\frac{\partial w_0(x,\theta)}{\partial x}\right) + A_{16}R^2\left(\frac{\partial^2 v_0(x,\theta)}{\partial x^2}\right) + A_{66}\left(\frac{\partial^2 u_0(x,\theta)}{\partial\theta^2}\right)$$

$$+B_{66}\left(\frac{\partial^2\phi_x(x,\theta)}{\partial\theta^2}\right)+A_{62}\left(\frac{\partial^2 v_0(x,\theta)}{\partial\theta^2}\right)+B_{16}R^2\left(\frac{\partial^2\phi_\theta(x,\theta)}{\partial x^2}\right)+B_{62}\left(\frac{\partial^2\phi_\theta(x,\theta)}{\partial\theta^2}\right)$$
$$+A_{62}\left(\frac{\partial w_0(x,\theta)}{\partial\theta}\right)\Bigg]=0, \tag{7a}$$

$$\frac{1}{R^2}\Bigg[R(B_{66}+B_{21})\left(\frac{\partial^2\phi_x(x,\theta)}{\partial x\partial\theta}\right)+R(B_{62}+B_{26})\left(\frac{\partial^2\phi_\theta(x,\theta)}{\partial x\partial\theta}\right)+R(A_{66}+A_{21})\left(\frac{\partial^2 u_0(x,\theta)}{\partial x\partial\theta}\right)$$
$$+R(A_{62}+A_{26})\left(\frac{\partial^2 v_0(x,\theta)}{\partial x\partial\theta}\right)+B_{26}\left(\frac{\partial^2\phi_x(x,\theta)}{\partial\theta^2}\right)+B_{22}\left(\frac{\partial^2\phi_\theta(x,\theta)}{\partial\theta^2}\right)+A_{26}\left(\frac{\partial^2 u_0(x,\theta)}{\partial\theta^2}\right)$$
$$+A_{22}\left(\frac{\partial^2 v_0(x,\theta)}{\partial\theta^2}\right)+B_{61}\left(\frac{\partial^2\phi_x(x,\theta)}{\partial x^2}\right)R^2+B_{66}R^2\left(\frac{\partial^2\phi_\theta(x,\theta)}{\partial x^2}\right)+A_{61}\left(\frac{\partial^2 u_0(x,\theta)}{\partial x^2}\right)R^2 \tag{7b}$$
$$+A_{66}R^2\left(\frac{\partial^2 v_0(x,\theta)}{\partial x^2}\right)+(k_sA_{44}+A_{22})\left(\frac{\partial w_0(x,\theta)}{\partial\theta}\right)+R(A_{45}k_s+A_{62})\left(\frac{\partial w_0(x,\theta)}{\partial x}\right)$$
$$+k_s\left(A_{45}R\phi_x(x,\theta)+A_{44}\left(\phi_\theta(x,\theta)R-v_0(x,\theta)\right)\right)\Bigg]=0,$$

$$\frac{1}{R^2}\Bigg[R^2(k_sA_{55}-N_a)\left(\frac{\partial^2 w_0(x,\theta)}{\partial x^2}\right)+k_sA_{44}\left(\frac{\partial^2 w_0(x,\theta)}{\partial\theta^2}\right)+2k_sRA_{45}\left(\frac{\partial^2 w_0(x,\theta)}{\partial x\partial\theta}\right)$$
$$+(k_sRA_{45}-B_{26})\left(\frac{\partial\phi_x(x,\theta)}{\partial\theta}\right)+(k_sRA_{44}-B_{22})\left(\frac{\partial\phi_\theta(x,\theta)}{\partial\theta}\right)+(-A_{22}-k_sA_{44})$$
$$\left(\frac{\partial v_0(x,\theta)}{\partial\theta}\right)+R(-B_{21}+Rk_sA_{55})\left(\frac{\partial\phi_x(x,\theta)}{\partial x}\right)+R(k_sRA_{45}-B_{26})\left(\frac{\partial\phi_\theta(x,\theta)}{\partial x}\right) \tag{7c}$$
$$-R(A_{45}k_s+A_{26})\left(\frac{\partial v_0(x,\theta)}{\partial x}\right)-A_{26}\left(\frac{\partial u_0(x,\theta)}{\partial\theta}\right)-A_{22}w_0(x,\theta)-A_{21}\left(\frac{\partial u_0(x,\theta)}{\partial x}\right)R\Bigg]=0,$$

$$\frac{1}{R^2}\Bigg[R(D_{16}+D_{61})\left(\frac{\partial^2\phi_x(x,\theta)}{\partial x\partial\theta}\right)+R(D_{12}+D_{66})\left(\frac{\partial^2\phi_\theta(x,\theta)}{\partial x\partial\theta}\right)+R(B_{16}+B_{61})\left(\frac{\partial^2 u_0(x,\theta)}{\partial x\partial\theta}\right)$$
$$+R(B_{12}+B_{66})\left(\frac{\partial^2 v_0(x,\theta)}{\partial x\partial\theta}\right)+D_{66}\left(\frac{\partial^2\phi_x(x,\theta)}{\partial\theta^2}\right)D_{62}\left(\frac{\partial^2\phi_\theta(x,\theta)}{\partial\theta^2}\right)+B_{66}\left(\frac{\partial^2 u_0(x,\theta)}{\partial\theta^2}\right)$$
$$+B_{62}\left(\frac{\partial^2 v_0(x,\theta)}{\partial\theta^2}\right)+D_{11}\left(\frac{\partial^2\phi_x(x,\theta)}{\partial x^2}\right)R^2+D_{16}R^2\left(\frac{\partial^2\phi_\theta(x,\theta)}{\partial x^2}\right)+B_{11}\left(\frac{\partial^2 u_0(x,\theta)}{\partial x^2}\right)R^2 \tag{7d}$$
$$+B_{16}R^2\left(\frac{\partial^2 v_0(x,\theta)}{\partial x^2}\right)+(-k_sRA_{45}+B_{62})\left(\frac{\partial w_0(x,\theta)}{\partial\theta}\right)-R\Bigg((-B_{12}+Rk_sA_{55})\left(\frac{\partial w_0(x,\theta)}{\partial x}\right)$$
$$+k_s\left(RA_{55}\phi_x(x,\theta)+A_{45}\left(\phi_\theta(x,\theta)R-v_0(x,\theta)\right)\right)\Bigg)\Bigg]=0,$$

$$\frac{1}{R^2}\Bigg[R(D_{66}+D_{21})\left(\frac{\partial^2\phi_x(x,\theta)}{\partial x\partial\theta}\right)+R(D_{62}+D_{26})\left(\frac{\partial^2\phi_\theta(x,\theta)}{\partial x\partial\theta}\right)+R(B_{66}+B_{21})\left(\frac{\partial^2 u_0(x,\theta)}{\partial x\partial\theta}\right)$$
$$+R(B_{62}+B_{26})\left(\frac{\partial^2 v_0(x,\theta)}{\partial x\partial\theta}\right)+D_{26}\left(\frac{\partial^2\phi_\theta(x,\theta)}{\partial\theta^2}\right)+D_{22}\left(\frac{\partial^2\phi_\theta(x,\theta)}{\partial\theta^2}\right)+B_{26}\left(\frac{\partial^2 u_0(x,\theta)}{\partial\theta^2}\right)$$
$$+B_{22}\left(\frac{\partial^2 v_0(x,\theta)}{\partial\theta^2}\right)+D_{61}\left(\frac{\partial^2\phi_x(x,\theta)}{\partial x^2}\right)R^2+D_{66}R^2\left(\frac{\partial^2\phi_\theta(x,\theta)}{\partial x^2}\right)+B_{61}\left(\frac{\partial^2 u_0(x,\theta)}{\partial x^2}\right)R^2 \tag{7e}$$
$$+B_{66}R^2\left(\frac{\partial^2 v_0(x,\theta)}{\partial x^2}\right)+(-k_sA_{44}R+B_{22})\left(\frac{\partial w_0(x,\theta)}{\partial\theta}\right)-R\Bigg((-B_{62}+k_sRA_{45})\left(\frac{\partial w_0(x,\theta)}{\partial x}\right)$$
$$+k_s\left(A_{45}R\phi_x(x,\theta)+A_{44}\left(\phi_\theta(x,\theta)R-v_0(x,\theta)\right)\right)\Bigg)\Bigg]=0.$$

3. Solution method

Using Navier solution method, the steady state solution of the governing equations obtained for the FML cylindrical shell (i.e., Eq. (7)) with simply-supported boundary conditions can be assumed as

$$u_0(x,\theta)=U_0\cos\left(\frac{m\pi x}{L}\right)\cos(n\theta/2),\qquad v_0(x,\theta)=V_0\sin\left(\frac{m\pi x}{L}\right)\sin(n\theta/2),$$
$$w_0(x,\theta)=W_0\sin\left(\frac{m\pi x}{L}\right)\cos(n\theta/2),\quad \phi_x(x,\theta)=\psi_1\cos\left(\frac{m\pi x}{L}\right)\cos(n\theta/2), \tag{8}$$
$$\phi_\theta(x,\theta)=\psi_2\sin\left(\frac{m\pi x}{L}\right)\sin(n\theta/2).$$

where m is the axial half wave number and n is the circumferential half wave number that for simplifying the equations $n'=n/2$ will be considered where n' is circumferential wave number. Substituting Eq. (8) into Eq. (7) gives the following equation for FSDT

$$\begin{bmatrix} L_1 & L_2 & L_3 & L_4 & L_5\\ L_6 & L_7 & L_8 & L_9 & L_{10}\\ L_{11} & L_{12} & L_{13} & L_{14} & L_{15}\\ L_{16} & L_{17} & L_{18} & L_{19} & L_{20}\\ L_{21} & L_{22} & L_{23} & L_{24} & L_{25}\end{bmatrix}\begin{bmatrix} U_0\\ V_0\\ W_0\\ \psi_1\\ \psi_2\end{bmatrix}=0 \tag{9}$$

where L_i (i=1...25) are given in Appendix A. Eq. (9) can be simplified based on the CLT

$$\begin{bmatrix} L_1 & L_2 & L_3\\ L_4 & L_5 & L_6\\ L_7 & L_8 & L_9\end{bmatrix}\begin{bmatrix} U_0\\ V_0\\ W_0\end{bmatrix}=0. \tag{10}$$

Table 2 Mechanical properties of unidirectional composite plies (Ungbhakorn and Singhatanadgid 2003)

Materials	E_{11}, GPa	E_{22}, GPa	G_{12}, GPa	υ_{12}
Graphite/Epoxy	132	10.8	5.65	0.24
Kevlar/Epoxy	76.8	5.5	2.07	0.34
E-glass/Epoxy	38.8	8.27	4.14	0.26

Table 3 Comparison of buckling loads (N/mm) of a metallic cylinder for R=L=1000 mm, h=3 mm and n'=0

m	Ugural (1981)	Present study	
		CLT	FSDT
1	20944.82	20945	20945
2	5242.692	5242.7	5242.7
3	2342.58	2342.6	2342.6
4	1336.623	1336.6	1336.6
5	880.9742	880.9742	880.9451
6	644.0334	644.0334	643.9731
7	512.1813	512.1813	512.0696
8	437.9575	437.9575	437.767
9	398.6888	398.6888	398.3838
10	382.4335	382.4335	381.969

where L_i (i=1...9) are given in Appendix B. To solve the Eqs. (9) and (10), the determinant of coefficient matrix should be zero and consequently the buckling load is obtained. It should be noted that Eqs. (9) and (10) do not give the critical buckling load (minimum buckling load) directly. For specific values of material properties and geometry parameters, many buckling loads are obtained for every value of m and n. The minimum load is selected as the critical buckling load. The critical buckling load does not happen at m=n' =1 essentially. Therefore, by changing the material properties and geometry parameters, this process should be repeated to obtain the critical buckling load.

4. Results and discussion

4.1 Validation of the proposed model

In order to validate the developed approach, the FML cylindrical shell is simplified to a full-metal cylindrical shell (MVF=1) and a full-composite cylindrical shell (MVF=0). Results obtained from the both CLT and FSDT are compared with those analytical results available in the literature. In the case of MVF=1, mechanical properties of aluminum are provided from Sadd (2009) as E=68.9 GPa, υ=0.34, and G=25.7 GPa. In the case of MVF=0, mechanical properties of various unidirectional composite plies are reported in Table 2.

Table 3 compares the buckling loads of a metallic circular cylindrical shell (MVF=1) obtained based on the CLT and FSDT in this study with results of those obtained based on CLT for simply-supported boundary conditions provided from Ugural (1981). Also, the buckling loads of a simply-

Table 4 Comparison of buckling loads (N/mm) of a composite cylinder based on the CLT for R=L=200 mm

Materials	m	n'	Ungbhakorn and Singhatanadgid (2003)	Present study (CLT)	Difference (%)
Graphite/Epoxy	3	11	84.23	84.0634	0.1978
Kevlar/Epoxy	3	11	39.38	39.3008	0.2011
E-glass/Epoxy	3	11	42.97	42.9697	0.698e-3

Table 5 Comparison of buckling loads (N/mm) of a composite cylinder based on the FSDT for R=200 mm

Materials	L/R	(m, n')	Ungbhakorn and Singhatanadgid (2003)	Present study (FSDT)	Difference (%)
Graphite/Epoxy	1	(3,11)	84.23	83.6718	0.66271
	2	(6,11)	84.23	83.6718	0.66271
	3	(9,11)	84.23	83.6718	0.66271
Kevlar/Epoxy	1	(3,10)	39.38	39.0699	0.78746
	2	(5,10)	38.96	38.6242	0.86191
	3	(8,10)	38.87	38.5547	0.81117
E-glass/Epoxy	1	(3,12)	42.97	42.8219	0.34466
	2	(6,12)	42.97	42.8219	0.34466
	3	(9,12)	42.97	42.8219	0.34466

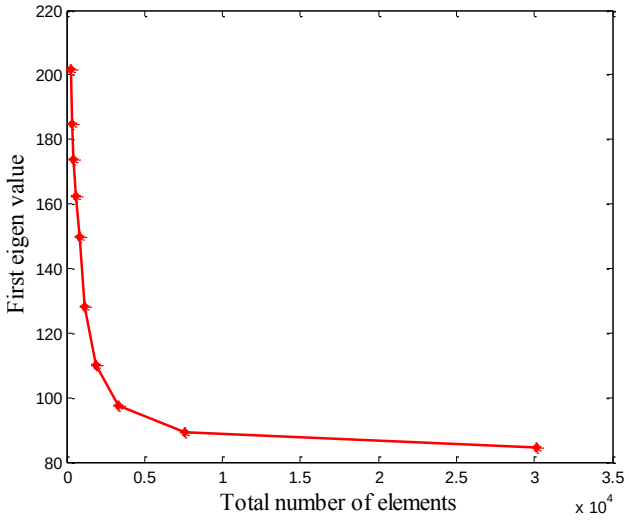

Fig. 3 Convergence for first eigenvalue vs. numbers of elements

supported composite cylindrical shell (MVF=0) with stacking sequence of $[0^{\circ}/90^{\circ}]_{2s}$ and ply thickness of t_{ply}=0.127 mm are obtained based on the developed approach in this study using CLT and FSDT and compared with results provided from Ungbhakorn and Singhatanadgid (2003) in Table 4 and 5. Results showed that the developed method in this study predicts the buckling loads of both metallic and composite cylinders with good accuracy at different longitudinal and

Table 6 Material properties used for FML cylindrical shell (Payeganeh *et al.* 2010)

Material	E_{11}, GPa	$E_{22}=E_{33}$, GPa	$G_{12}=G_{13}$, GPa	G_{23}, GPa	$\upsilon_{12}=\upsilon_{13}$
Glass/polyster	24.51	7.77	3.34	1.34	0.078
Al 2024-T3	72.4	72.4	27.6	27.6	0.33

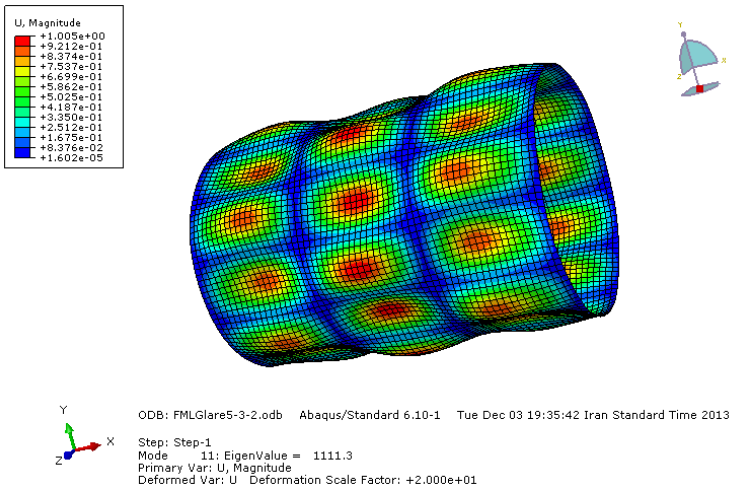

Fig. 4 Eleventh eigenvalue and buckling mode of GLARE 5 3/2

Table 7 Buckling loads (N/mm) of a FML cylinder with MVF=0.4 obtained from theory (using FSDT) and ABAQUS for GLARE 5 3/2 (R=200 mm, L=600mm, h=3 mm, k_s=5/6)

m	n'	ABAQUS	FSDT	Difference (%)
2	5	1086.7	1127.2	3.592974
6	7	1106.9	1118.2	1.010553
4	6	1110.6	1130.3	1.7429
3	6	1111.3	1133.6	1.967184
8	7	1112.2	1124.9	1.128989

circumferential modes.

4.2 Analytical and FE estimations of buckling loads of a FML cylindrical shell

Now the validation of the developed approach is confirmed by full-metal and full-composite cylindrical shells, the buckling behavior of a FML cylinder can be investigated analytically. In this study, the buckling loads of FML cylinders are also computed by finite element method. A simply-supported FML cylindrical shell is modeled in commercial finite element software, ABAQUS, and buckling loads are calculated by the linear eigenvalue analysis. Linear quadrilateral elements, S4R, are used to mesh the cylinder. Mesh sensitivity is done to obtain the appropriate element size. Fig. 3 shows the variation of first eigenvalue versus the total numbers of elements in the model. The appropriate element size is 5 mm. The material properties of FML are listed in Table 6. Fig. 4 shows the buckling mode of eleventh eigenvalue for instance related to m=3 and n'=6. Table 7

presents the buckling loads of a FML cylinder with MVF=0.4 obtained from FSDT and finite element method for GLARE 5 3/2. The maximum difference between analytical and numerical linear eigenvalue buckling loads are less than 4%.

4.3 Effect of different parameters of a FML cylindrical shell on the buckling loads

In this section, the effects of FML parameters such as MVF, stacking sequence of layers, types of layup (metal or composite), and geometric parameters is analytically investigated on buckling loads of a FML cylindrical shell based on the FSDT. Fig. 5 shows the variation of the buckling load versus the different values of circumferential half wave number (n) and m=1 for different values of MVF in GLARE 5 3/2 FML. The buckling load increases with increasing MVF from 0 to 1 for all the circumferential half wave number. This is due to increasing of FML stiffness with increasing MVF values. The buckling loads corresponded to$0 \leq MVF \leq 1$ lie between those of full-composite and full-metal shells. It is worth to note that the critical mode is observed in m=1 and n=8 for all MVF values. Also, the difference among the buckling loads in the case of FML and the in case of full-composite (MVF=0) is significant. It should be noted that similar results are approximately established for different types of GLARE. Fig. 6 depicts the effects of MVF on the buckling load of a FML cylindrical shell with L=600 mm and R=200 mm versus the axial half wave number (m) and n=2 for GLARE 5 3/2. Critical mode occurs in the higher axial half wave number than that of circumferential half wave number. Also, the variation of buckling loads versus the circumferential half wave number is more significant than the axial half wave number.

Fig. 7 illustrates the effect of different layups on the buckling loads of GLARE 5 FML shell versus MVF. It is obvious that by increasing the number of layers with constant thickness and

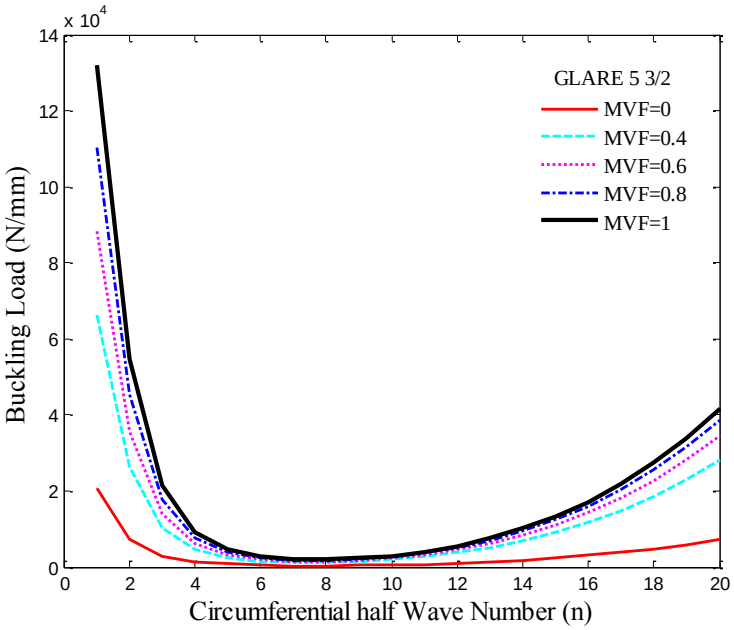

Fig. 5 Effect of MVF on the buckling loads vs. circumferential half wave number for GLARE 5 3/2 (L=600 mm, R=200 mm, m=1, h=3 mm)

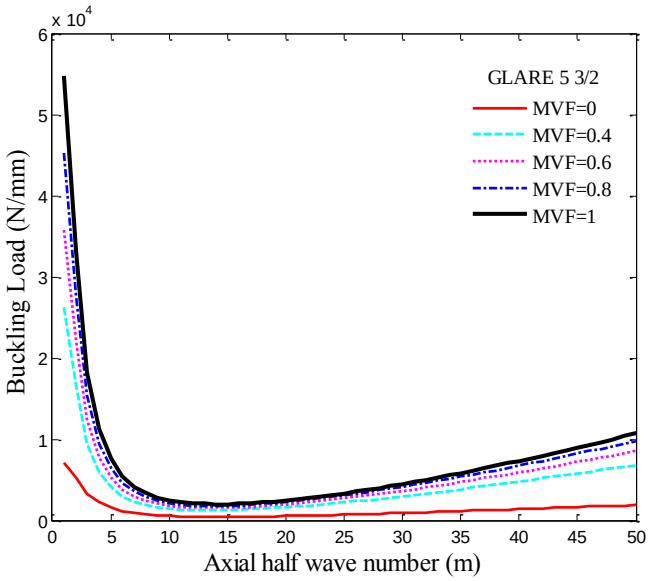

Fig. 6 Effect of MVF on the buckling load vs. axial half wave number for GLARE 5 3/2 (L=600 mm, R=200 mm, n=2, h=3 mm)

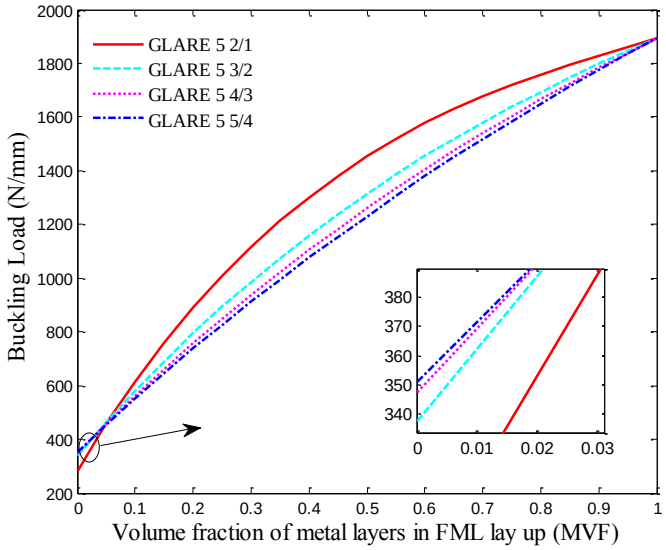

Fig. 7 Effect of layup on buckling loads of GLARE 5 vs. MVF (L=600 mm, R=200 mm, h=3 mm, m=1, n=8)

MVF, the buckling load approaches to a constant value. It is also observed from this figure, comparison between the values of buckling loads for $0 \leq \text{MVF} < 0.05$ with those for MVF> 0.05 reveals that the order of buckling load with respect to different layups is reversed.

Effects of radius of the shell on the buckling loads of different types of GLARE are plotted in Fig. 8. Results show that with increasing the shell radius up to 300 mm the buckling load increases

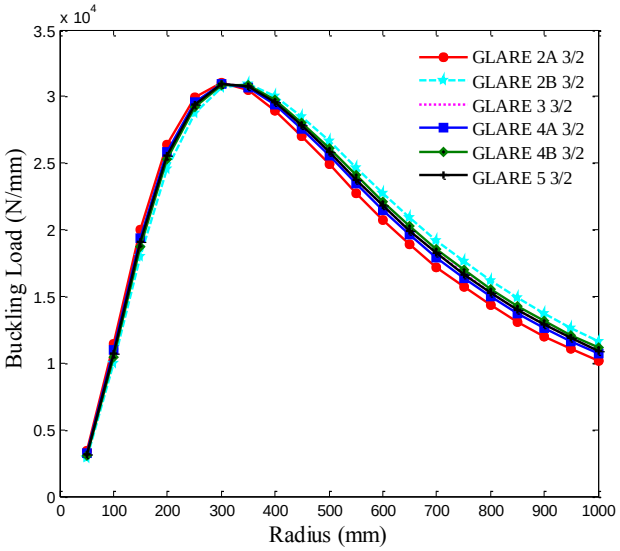

Fig. 8 Effect of shell radius on the buckling loads of different types of GLAREs (L=1000 mm, h=3 mm, m=1, n=2, MVF=0.5)

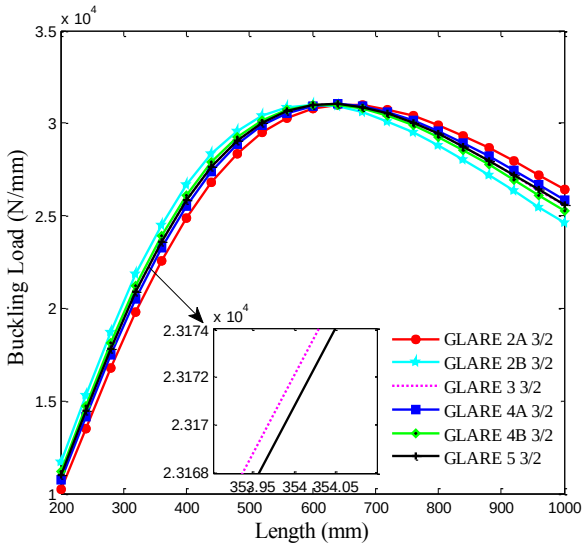

Fig. 9 Effect of shell length on the buckling loads of different types of GLAREs (R=200 mm, h=3 mm, m=1, n=2, MVF=0.5)

and it decreases after R=300 mm. Also, the effects of various types of GLAREs on the buckling loads become more distinguished at higher radius. As it is seen, comparison between the values of buckling loads for R<300 mm with those of R>300 mm reveals that the order of buckling load with respect to different GLAREs is reversed.

Fig. 9 illustrates the effects of length of the cylindrical shell on the buckling loads of different types of GLAREs. By increasing the shell length up to 625 mm the buckling load increases and

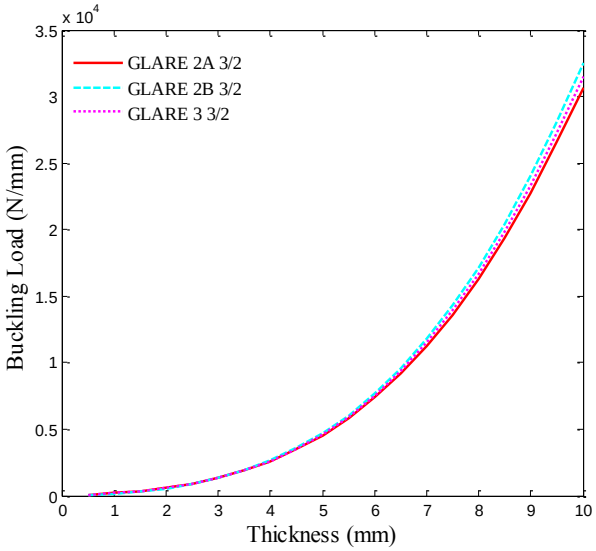

Fig. 10 Effect of cylindrical shell thickness on the buckling load of GLARE 2A, GLARE 2B and GLARE 3 (R=200 mm, L=600 mm, m=1, n=8, MVF=0.5)

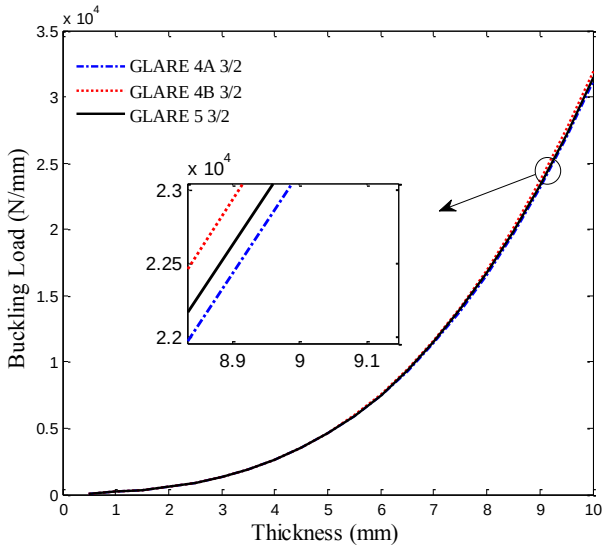

Fig. 11 Effect of cylindrical shell thickness on the buckling load of GLARE 4A, GLARE 4B and GLARE 5 (R=200 mm, L=600 mm, m=1, n=8, MVF=0.5)

then it decreases. It is also worth to mention that comparison the values of buckling loads of L<625mm with those of L>625 mm reveals that the order of buckling loads with respect to different GLAREs is reversed.

Effects of cylindrical shell thickness on the buckling loads of different types of GLAREs are demonstrated in Fig. 10 and Fig. 11. It is found that the buckling load increases by increasing the shell thickness and variation of the buckling load for all types of GLARE is more severe at higher

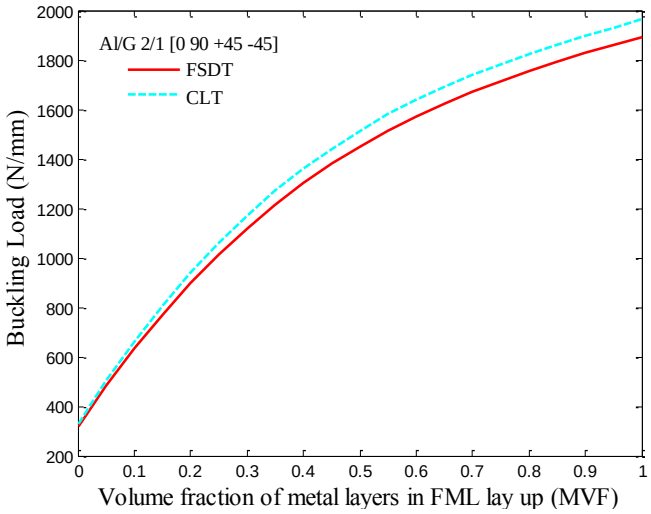

Fig. 12 Comparison of FSDT and CLT on prediction of the buckling loads vs. MVF (L=600 mm, R=200 mm, h=3 mm, m=1, n=8)

thicknesses. Obviously, the difference between the buckling loads of different types of GLAREs is larger at thick shells. It is also concluded that the maximum value of the buckling load is related to GLARE 2B and the minimum value is related to GLARE 2A at a constant thickness.

Fig. 12 depicts the variation of buckling loads calculated by CLT and FSDT versus MVF for a FML cylindrical shell with layup Al/G 2/1 and fibers orientation [0/90/+45/-45]. The difference between the buckling loads of FSDT and CLT is larger at higher MVF. It means that the FSDT gives more reliable results for buckling loads than CLT by increasing the value of MVF.

5. Conclusions

FML circular cylindrical shells due to their specific features are widely extended in different industries, especially aerospace industry. In this study, the buckling analysis of a FML cylindrical shell under axial compression load is investigated both analytically and numerically. For the first time, the governing equations for the buckling behavior of a FML circular cylindrical shell are derived based on the first-order shear deformation theory (FSDT) and solved by Navier solution for simply-supported boundary conditions. Also, a FML cylindrical shell is modeled in the commercial finite element software, ABAQUS, and buckling loads are calculated numerically by the linear eigenvalue buckling analysis. Analytical and numerical results are compared with each other and verified with available results in the literature for the special cases such as full-metallic and full-composite cylindrical shells. To show the efficiency of FML materials rather than other materials used in aerospace industry, different parameters of FML such as metal volume fraction (MVF), stacking sequence of layers, types of layers (composite or metal), and geometric parameters are discussed in detail on the buckling loads of cylindrical shells. Results indicate that the metal layer is an effective controlling parameter for buckling loads of the FML cylindrical shells. It is found that the buckling load increases by increasing of MVF for all circumferential half wave numbers and axial half wave numbers. By increasing the number of layers and MVF in

a constant thickness, the buckling load approaches to a constant value. Also, by increasing shell radius and length, the buckling load first increases and then it decreases. It is also observed that the difference between the buckling loads of different types of GLAREs is larger at thick shell and the maximum value of the buckling load is related to GLARE 2B and the minimum is related to GLARE 2A (for a constant thickness). Finally, it is hoped that the results presented in this paper would be helpful for study and design of FML cylindrical shells.

References

Botelho, E.C., Silva, R.A., Pardini, L.C. and Rezende, M.C. (2006), "A review on the development and properties of continuous fiber/epoxy/aluminum hybrid composites for aircraft structures", *Mater Res*., **9**, 247-256.

Carrillo, J.G. and Cantwell, W.J. (2007), "Scaling effects in the tensile behavior of fiber-metal laminates", *Compos. Sci. Technol*., **67**, 1684-1693.

Fan, H.G., Chen, Z.P., Feng, W.Z., Zhou, F., Shen, X.L., Cao, G.W. (2015), "Buckling of axial compressed cylindrical shells with stepwise variable thickness", *Struct. Enging. Mech*., **54**(1), 87-103.

Heidari-Rarani, M., Khalkhali-Sharifi, S.S., Shokrieh, M.M. (2014), "Effect of ply stacking sequence on buckling behavior of E-glass/epoxy laminated composites", *Comput. Mater. Sci*., **89**, 89-96.

Hosseini Hashemi, S.H., Atashipour, S.R., Fadaee, M. and Girhammar, U.A. (2012), "An exact closed form procedure for free vibration analysis of laminated spherical shell panels based on Sanders theory", *Arch. Appl. Mech*., **82**, 985-1002.

Kardomateas, G.A. (1996), "Benchmark three dimensional elasticity solutions for the buckling of thick orthotropic cylindrical shells", *Compos. Part B*, **27**, 569-580.

Khalili, S.M.R., Malekzadeh, K., Davar, A. and Mahajan, P. (2010), "Dynamic response of pre-stressed fibre metal laminate (FML) circular cylindrical shells subjected to lateral pressure pulse loads", *Compos. Struct*., **92**, 1308-1317.

Khdeir, A.A., Reddy, J.N. and Frederick, D.A. (1989), "study of bending, vibration and buckling of cross-ply circular cylindrical shells with various shell theories", *Int. J. Eng. Sci*., **27**, 1337-1351.

Krishnakumar, S. (1994), "Fiber metal laminates–the synthesis of metals and composites", *Mater Manuf. Pr.*, **9**, 295-354.

Li, X. and Chen, Y. (2002), "Transient dynamic response analysis of orthotropic circular cylindrical shell under external hydrostatic pressure", *J. Sound Vib*., **257**, 967-976.

Mandal, P. and Calladine, C.R. (2000), "Buckling of thin cylindrical shells under axial compression", *Int. J. Solid. Struct*., **37**, 4509-4525.

Nam, H.W., Jung, S.W., Jung, C.K. and Han, K.S. (2003), "A model of damage initiation in singly oriented ply fiber metal laminate under concentrated loads", *J. Compos. Mater*, **37**, 269-281.

Payeganeh, G.H., Ghasemi, F.A. and Malekzadeh, K. (2010), "Dynamic responseof fiber metal laminates (FMLs) subjected to low-velocity impact", *Thin Wall Struct.*, **48**, 62-70.

Reddy, J.N. (2003), *Mechanics of laminated composite plates and shells: theory and analysis*, CRC Press, New York.

Sadd, M.H., (2009), *Elasticity Theory, Applications and Numerics*, Elsevier Inc, USA.

Shen Shen, H. and Xiang, Y. (2008), "Buckling and post buckling of anisotropic laminated cylindrical shells under combined axial compression and torsion", *Compos. Struct*., **84**, 375-386.

Shi, G. and Xiong, Y. (2000), "Probabilistic buckling analysis of fiber metal laminates under shear loading condition", *Adv. Eng. Softw*., **31**, 519-527.

Silvestre, N. (2008), "Buckling behaviour of elliptical cylindrical shells and tubes under compression", *Int. J. Solid. Struct*., **45**, 4427-4447.

Sinmazçelik, T., Avcu, E., Özgür Bora, M. and Çoban, O. (2011), "A review: Fibre metal laminates, background, bonding types and applied test methods", *Mater. Des*., **32**, 3671-3685.

Tahir, Z.R. and Mandal, P. (2012), "A new perturbation technique in numerical study on buckling of composite shells under axial compression", *World Acad. Sci. Eng. Technol.*, **70**, 10-27.
Topal, U. and Uzman, V. (2009), "Thermal buckling load optimization of angle-ply laminated cylindrical shells", *Mater. Des.*, **30**, 532-536.
Tvergaard, V. and Needleman, A. (2000), "Buckling localization in a cylindrical panel under axial compression", *Int. J. Solid. Struct.*, **37**, 6825-6842.
Ugural, A.C. (1981), *Stresses in plate and shells*, McGraw-Hill, USA.
Ungbhakorn, V. and Singhatanadgid, P. (2003), "Similitude and physical modeling for buckling and vibration of symmetric cross-ply laminated circular cylindrical shells", *J. Compos. Mater.*, **37**, 1697-1712.
Vinson, J.R. (1993), *The mechanical behaviour of shells composed of isotropic and composite materials*, Kluwer academic publishers, Dordrecht (Boston, London).
Vlot, A., Alderliesten, R., Hooijmeijer, P., de Kanter, J., Sinke, J. and Ypma, M. (2002), "Fibre metal laminates: a state of the art", *Int. J. Mater. Prod. Technol.*, **17**, 79-98.
Vlot, A. and Gunnink, J.W. (2001), *Fibre metal laminates-an introduction*, Kluwer Academic Publishers, Dordrecht, Boston, London.

CC

Appendix A

$$L_1=\frac{(-n'^2L^2A_{66}-A_{11}m^2\pi^2R^2)}{L^2R^2},\ L_2=\frac{(A_{12}m\pi LRn'+nLA_{66}m\pi R)}{L^2R^2},\ L_3=\frac{A_{12}m\pi}{LR},$$

$$L_4=\frac{(-B_{11}m^2\pi^2R^2-n'^2L^2B_{66})}{L^2R^2},L_5=\frac{(B_{12}m\pi n'LR+n'LB_{66}m\pi R)}{L^2R^2},\ L_6=\frac{(A_{12}m\pi LRn'+n'LA_{66}m\pi R)}{L^2R^2},$$

$$L_7=\frac{(-n'^2L^2A_{22}-A_{66}m^2\pi^2R^2-k_sA_{44}L^2)}{L^2R^2},\ L_8=\frac{(-k_sA_{44}L^2n'-n'L^2A_{22})}{L^2R^2},$$

$$L_9=\frac{(B_{12}m\pi n'LR+n'LB_{66}m\pi R)}{L^2R^2},\ L_{10}=\frac{(-n'^2L^2B_{22}-B_{66}m^2\pi^2R^2+k_sA_{44}L^2R)}{L^2R^2},\ L_{11}=\frac{A_{12}m\pi}{LR},$$

$$L_{12}=\frac{(-k_sA_{44}L^2n'-n'L^2A_{22})}{L^2R^2},\ L_{13}=\frac{(-k_sA_{44}L^2n'^2-k_sA_{55}m^2\pi^2R^2-A_{22}L^2+N_am^2\pi^2R^2)}{L^2R^2},$$

$$L_{14}=\frac{(LB_{12}m\pi R-k_sA_{55}m\pi R^2L)}{L^2R^2},\ L_{15}=\frac{(k_sA_{44}L^2n'R-B_{22}n'L^2)}{L^2R^2},\ L_{16}=\frac{(-B_{11}m^2\pi^2R^2-n'^2L^2B_{66})}{L^2R^2},$$

$$L_{17}=\frac{(B_{12}m\pi n'LR+n'LB_{66}m\pi R)}{L^2R^2},\ L_{18}=\frac{(LB_{12}m\pi R-k_sA_{55}m\pi R^2L)}{L^2R^2},$$

$$L_{19}=\frac{(-D_{11}m^2\pi^2R^2-n'^2L^2D_{66}-k_sA_{55}L^2R^2)}{L^2R^2},\ L_{20}=\frac{(D_{12}m\pi n'LR+n'LD_{66}m\pi R)}{L^2R^2},$$

$$L_{21}=\frac{(B_{12}m\pi n'LR+n'LB_{66}m\pi R)}{L^2R^2},\ L_{22}=\frac{(-n'^2L^2B_{22}-B_{66}m^2\pi^2R^2+k_sA_{44}L^2R)}{L^2R^2},$$

$$L_{23}=\frac{(k_sA_{44}L^2n'R-B_{22}n'L^2)}{L^2R^2},\ L_{24}=\frac{(D_{12}m\pi n'LR+n'LD_{66}m\pi R)}{L^2R^2},$$

$$L_{25}=\frac{(-n'^2L^2D_{22}-D_{66}m^2\pi^2R^2-k_sA_{44}L^2R^2)}{L^2R^2}.$$

Appendix B

$$L_1=\frac{(-A_{11}m^2\pi^2LR^2-n'^2L^3A_{66})}{L^3R^2},\ L_2=\frac{(n'L^2A_{66}m\pi R+A_{12}m\pi L^2Rn')}{L^3R^2},$$

$$L_3=\frac{(B_{12}m\pi n'^2L^2+2n'^2L^2B_{66}m\pi+A_{12}m\pi L^2R+B_{11}m^3\pi^3R^2)}{L^3R^2},$$

$$L_4=\frac{(n'R^3A_{12}m\pi L+m\pi R^2B_{66}n'L+A_{66}m\pi R^3n'L+n'B_{12}m\pi LR^2)}{L^2R^4},$$

$$L_5=\frac{(-A_{66}m^2\pi^2R^4-n'^2R^2A_{22}L^2-m^2\pi^2R^3B_{66}-B_{22}L^2Rn'^2)}{L^2R^4},$$

$$L_6 = \left(\frac{-n' D_{12} m^2 \pi^2 R^2 - 2B_{66} m^2 \pi^2 n' R^3 - n'^3 R B_{22} L^2 - n' R^2 A_{22} L^2}{L^2 R^4} \right.$$

$$\left. + \frac{-n' R^3 B_{12} m^2 \pi^2 - D_{22} n'^3 L^2 - n' B_{22} L^2 R - 2m^2 \pi^2 R^2 n' D_{66}}{L^2 R} \right),$$

$$L_7 = \frac{(B_{12} m\pi n'^2 L^3 R^2 + 2n'^2 L^3 R^2 B_{66} m\pi + A_{12} m\pi L^3 R^3 + B_{11} m^3 \pi^3 L R^4)}{L^4 R^4},$$

$$L_8 = \frac{(-L^4 R^2 A_{22} n' - B_{12} m^2 \pi^2 n' L^2 R^3 - n'^3 L^4 B_{22} R - 2m^2 \pi^2 n' L^2 R^3 B_{66})}{L^4 R^4},$$

$$L_9 = \left(\frac{-2D_{12} m^2 \pi^2 n'^2 L^2 R^2 - L^4 R^2 A_{22} - 2B_{12} m^2 \pi^2 L^2 R^3 - D_{11} m^4 \pi^4 R^4}{L^4 R^4} \right.$$

$$\left. + \frac{-2n'^2 L^4 B_{22} R - 4m^2 n'^2 \pi^2 L^2 R^2 D_{66} - n'^4 L^4 D_{22} + N_a m^2 \pi^2 L^2 R^4}{L^4 R^4} \right).$$